Curvature-induced domain wall pinning

Kostiantyn V. Yershov,[1,2,*] Volodymyr P. Kravchuk,[1,†] Denis D. Sheka,[3,‡] and Yuri Gaididei[1,§]
[1]*Bogolyubov Institute for Theoretical Physics, 03680 Kyiv, Ukraine*
[2]*National University of "Kyiv-Mohyla Academy", 04655 Kyiv, Ukraine*
[3]*Taras Shevchenko National University of Kyiv, 01601 Kyiv, Ukraine*
(Received 11 June 2015; published 14 September 2015)

It is shown that a local bend of a nanowire is a source of pinning potential for a transversal head-to-head (tail-to-tail) domain wall. Eigenfrequency of the domain wall free oscillations at the pinning potential and the effective friction are determined as functions of the curvature and domain wall width. The pinning potential originates from the effective curvature-induced Dzyaloshinsky-like term in the exchange energy. The theoretical results are verified by means of micromagnetic simulations for the case of parabolic shape of the wire bend.

DOI: 10.1103/PhysRevB.92.104412 PACS number(s): 75.10.Hk, 75.40.Mg, 75.60.Ch, 75.78.Fg

I. INTRODUCTION

Dynamics of domain walls in nanowires underlies modern memory [1,2] and logic [3–5] devices; see also review in Ref. [6]. Most of these designs require wires with curvilinear segments, e.g., vertical configuration of the racetrack magnetic memory [1]. Therefore, the modification of dynamic and static properties of a domain wall due to the wire curvature is of high importance for the applications. It is known that the local curvilinear defects of the wire can be a source of pinning potential for the domain wall [7–9]. However, in contrast to widely studied mechanisms of the domain wall pinning, such as interaction with artificial notches [10–17], surface roughnesses [18–21], and inhomogeneities in the magnetocrystalline anisotropy distribution [21–23], the role of the curvature remains unclear and the general theory is absent. Nevertheless, one should note some progress in studying the simplest case of circular wire geometry, where the domain wall pinning is achieved due to the applied external magnetic field [24,25].

As it was recently shown [26] the exchange interaction in a curvilinear wire can produce an effective Dzyaloshinsky-like term. In this paper we demonstrate that the inhomogeneous distribution of this curvature-induced Dzyaloshinsky-like contribution can be an origin of domain wall pinning at the local wire bend, analogous to the case of studied anisotropy inhomogeneities [21–23]. Considering the coordinate dependent curvature of the wire we propose a general approach valid for a wide class of geometries.

II. MODEL AND GENERAL RESULTS

In this paper we consider a plane curved ferromagnetic wire of circular cross section. Such a wire can be parametrized in the following way:

$$\boldsymbol{r}(s,\chi,\rho) = \boldsymbol{\gamma}(s) + \rho\,\cos\chi\,\boldsymbol{e}_{\mathrm{N}}(s) + \rho\,\sin\chi\,\boldsymbol{e}_{\mathrm{B}}(s). \qquad (1)$$

Here the three-dimensional radius vector $\boldsymbol{r}$ defines the space domain, occupied by the wire, the two-dimensional vector $\boldsymbol{\gamma}(s) = \gamma_x(s)\hat{\boldsymbol{x}} + \gamma_y(s)\hat{\boldsymbol{y}}$ determines the wire central line, which lies within the xy plane, with s being the natural parameter (arc length). Within a wire cross section the polar coordinates $\rho \in [0, R]$ and $\chi \in [0, 2\pi)$ are used, where R is the wire radius. We use here the Frenet-Serret basis $(\boldsymbol{e}_{\mathrm{T}}, \boldsymbol{e}_{\mathrm{N}}, \boldsymbol{e}_{\mathrm{B}})$ with $\boldsymbol{e}_{\mathrm{T}} = \boldsymbol{\gamma}'(s)$, $\boldsymbol{e}_{\mathrm{N}} = \boldsymbol{\gamma}''(s)/\kappa(s)$, and $\boldsymbol{e}_{\mathrm{B}} = \boldsymbol{e}_{\mathrm{T}} \times \boldsymbol{e}_{\mathrm{N}}$ being the tangential, normal, and binormal unit vectors, respectively. Here the wire curvature $\kappa(s) = |\boldsymbol{\gamma}''(s)|$ is introduced.

Using the Frenet-Serret basis one can introduce the angular magnetization parametrization

$$\boldsymbol{m} = \cos\theta\,\boldsymbol{e}_{\mathrm{T}} + \sin\theta\,\cos\phi\,\boldsymbol{e}_{\mathrm{N}} + \sin\theta\,\sin\phi\,\boldsymbol{e}_{\mathrm{B}}, \qquad (2)$$

where $\boldsymbol{m} = \boldsymbol{M}/M_s$ is the normalized magnetization unit vector with M_s being the saturation magnetization.

Magnetization dynamics of this system can be studied by means of phenomenological Landau-Lifshitz equations

$$-\sin\theta\dot{\theta} = \omega_0\frac{\delta\mathcal{E}}{\delta\phi} + \alpha\,\sin^2\theta\dot{\phi}, \quad \sin\theta\dot{\phi} = \omega_0\frac{\delta\mathcal{E}}{\delta\theta} + \alpha\dot{\theta}, \qquad (3)$$

where overdot indicates the time derivative, frequency $\omega_0 = 4\pi\gamma_0 M_s$ determines the characteristic time scale of the system with γ_0 being the gyromagnetic ratio, $\mathcal{E} = E/4\pi M_s^2$ is normalized total energy, and α is the damping coefficient.

We start with a simple model, which takes into account only two contributions to the total magnetic energy

$$\mathcal{E} = \mathcal{S}\int_{-\infty}^{+\infty}[\ell^2\mathscr{E}_{\mathrm{ex}} - k_{\mathrm{t}}\cos^2\theta]ds, \qquad (4)$$

namely, exchange one $\mathscr{E}_{\mathrm{ex}}$ and easy-tangential anisotropy—the second term in (4). Here $\mathcal{S} = \pi R^2$ is the area of the wire cross section, $\ell = \sqrt{A/4\pi M_s^2}$ is the exchange length with A being exchange constant, and $k_{\mathrm{t}} = K/(4\pi M_s^2) + 1/4$ is the dimensionless anisotropy constant. Here $K > 0$ is constant magnetocrystalline anisotropy of easy-tangential type and the term $1/4$ comes from the magnetostatic contribution. It is known [27–30] that for thin wires of circular and square cross sections the magnetostatic energy is reduced to an effective easy-tangential shape anisotropy with $K_{\mathrm{eff}} = \pi M_s^2$, including the case of a curvilinear wire [29]. Competition of the exchange and anisotropy contributions results in the length scale of the system $w = \ell/\sqrt{k_{\mathrm{t}}}$. For magnetically soft wires $K = 0$ and $w = 2\ell$. In (4) and everywhere below we restrict ourselves with the case of thin wire $R \lesssim w$; thus we assume that the

*yershov@bitp.kiev.ua
†vkravchuk@bitp.kiev.ua
‡sheka@univ.net.ua
§ybg@bitp.kiev.ua

 ©2015 American Physical Society

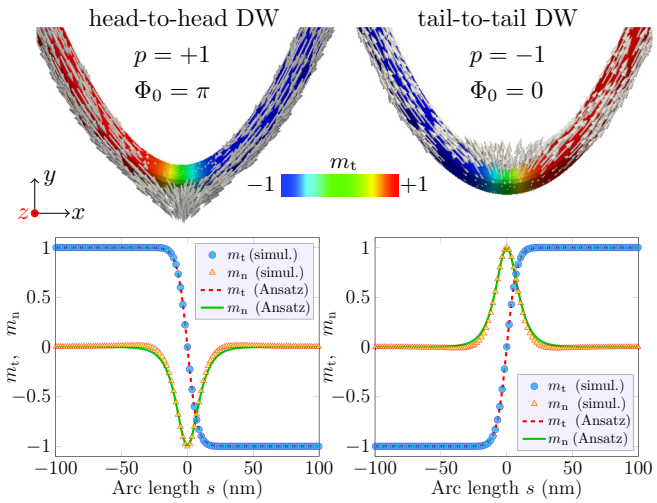

FIG. 1. (Color online) Equilibrium state of the transversal domain wall at the wire bend. Top row shows the magnetization distribution obtained using micromagnetic NMAG simulations for permalloy parabolic wire with $R = 5$ nm, total length $L = 1$ μm, and $\kappa_0 = 0.05$ nm^{-1} (only the bend vicinity is shown). The bottom row demonstrates comparison of magnetization components $m_t = \boldsymbol{m} \cdot \boldsymbol{e}_T$ and $m_n = \boldsymbol{m} \cdot \boldsymbol{e}_N$ obtained from the simulations (markers) and from the Ansatz (7) (lines). In the latter case the domain wall width $\Delta = 2\ell$ was used.

magnetization varies along the wire and it is uniform within a wire cross section: $\boldsymbol{m} = \boldsymbol{m}(s)$.

In terms of the angular parametrization (2) the exchange energy density has a form [26]

$$\mathcal{E}_{ex} = (\theta' + \kappa \cos\phi)^2 + (\phi' \sin\theta - \kappa \cos\theta \sin\phi)^2, \quad (5)$$

where the prime denotes derivative with respect to s. In (5) it is taken into account that a plane wire has zero torsion.

Let us first analyze static solutions of (3). In this case there is a solution $\phi = \phi_0 = 0, \pi$, which corresponds to a planar magnetization distribution: vectors $\boldsymbol{m}(s)$ lie within the wire plane. The corresponding function θ is determined by an inhomogeneous Sine-Gordon equation (for details, see Appendix A)

$$w^2\theta'' - \sin\theta \cos\theta = -w^2\kappa' \cos\phi_0. \quad (6)$$

For the case $\kappa' \equiv 0$ (rectilinear or circular wire) Eq. (6) has the well known domain wall solutions $\cos\theta = -p \tanh[(s - q)/\Delta]$ of head-to-head ($p = 1$) or tail-to-tail ($p = -1$) types. Here q determines the domain wall position and $\Delta = w$ is the wall width. For the case $\kappa' \not\equiv 0$ an additional driving force appears and the curvature-induced domain wall dynamics is expected. In the following, we consider a case of a localized curvature, i.e., $\kappa(\pm\infty) = 0$ and $\kappa'(\pm\infty) = 0$, see Figs. 1 and 2(a), this results in the boundary conditions $\cos\theta(\pm\infty) = \mp p$, the same as for a rectilinear wire. We also restrict ourselves with the case $w^2\kappa' \ll 1$ assuming that the domain wall retains its form and the curvature influence results in a weak modification of the width Δ. Therefore, to analyze the domain wall properties (static as well as dynamic ones) we use a collective variable approach [31,32] based on the simple q–Φ model [31,33]

$$\cos\theta = -p \tanh\left[\frac{s - q(t)}{\Delta}\right], \quad \phi = \Phi(t), \quad (7)$$

which is widely used for different types of domain walls and various drivings [19,20,27,34–40]. The domain wall position q and phase Φ, which determines orientation of the transversal magnetization component, make a canonically conjugated pair of collective variables. The domain wall width Δ is shown to be a slaved variable [27,37], i.e., $\Delta(t) = \Delta[q(t), \Phi(t)]$. However, this is not the case when Φ depends on the coordinate [41] (it is possible for a three dimensional wire, when the torsion is present); in this case a generalization of the $q-\Phi$ model [41] must be applied.

Substituting now the Ansatz (7) into (4) one obtains the total energy in the form (up to an additive constant)

$$\frac{\mathcal{E}}{2\mathcal{S}} = \left(\frac{\ell^2}{\Delta} + k_t\Delta\right) + \pi\ell^2 p \cos\Phi\kappa(q) - \ell^2\Delta \sin^2\Phi\kappa^2(q), \quad (8)$$

where the condition $\kappa\Delta \ll 1$ was applied when integrating (4); for details see Appendix B. The first term in (8) reflects the exchange-anisotropy competition which determines the domain wall width for a rectilinear wire. The second and the third terms originate from Dzyaloshinsky-like and anisotropylike terms, respectively, which effectively appear in the exchange energy due to the curvature [26]. Minimization of (8) with respect to parameters q and Φ results in the following

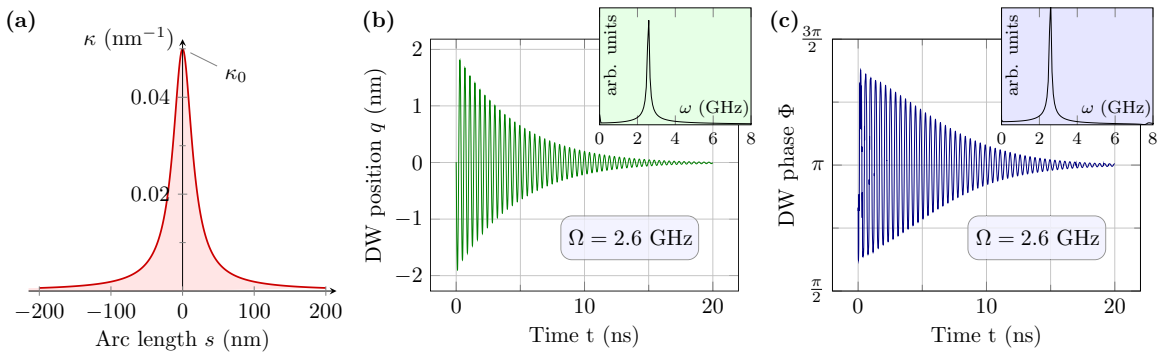

FIG. 2. (Color online) (a) Curvature of the parabolic wire (16) with $\kappa_0 = 0.05$ nm^{-1}. Insets (b) and (c) show the time dependences (with the corresponding Fourier spectra) of position $q(t)$ and phase $\Phi(t)$ of the domain wall, perturbed at vicinity of the equilibrium point $q_0 = 0$. The data are obtained by means of micromagnetic simulations for a wire with $\kappa_0 = 0.05$ nm^{-1} and $R = 5$ nm.

equilibrium values q_0 and Φ_0:

$$\kappa'(q_0) = 0, \quad \cos\Phi_0 = -p. \tag{9}$$

Thus the domain wall is pinned at the maximum of the curvature, and the phase selectivity takes place: the head-to-head domain wall is always directed outward while the tail-to-tail one is directed inward the bend; see Fig. 1. The latter effect was recently observed experimentally [17]. There is an intuitive explanation: the choice of Φ_0 defined by (9) makes the magnetization distribution more homogeneous, see Fig. 1, which decreases the exchange energy.

As it follows from (8), the equilibrium value of the domain wall width $\Delta_0 = w$ is the same as for a rectilinear wire. However, if the wall is perturbed and the values of quantities (q, Φ) deviate from the equilibrium (9), the domain wall width is modified as follows: $\Delta(q,\Phi) = \ell[k_t - k_b(q)\sin^2\Phi]^{-1/2}$, where $k_b = \ell^2\kappa^2(q)$ is coefficient of the curvature-induced effective easy-binormal anisotropy. The similar domain wall width modification caused by a geometrical constraint was discussed in Ref. [42].

As it follows from Fig. 1 the used Ansatz (7) and the obtained static results (9) are in a good agreement with the simulations results.

Let us now proceed to dynamical properties of the domain wall. In terms of the collective variables the equations of motion (3) take a form (see Appendix B)

$$\dot q = \frac{\omega_0}{2\mathcal{S}}\frac{\partial\mathcal{E}}{\partial\Phi} + \alpha\Delta\dot\Phi, \quad \dot\Phi = -\frac{\omega_0}{2\mathcal{S}}\frac{\partial\mathcal{E}}{\partial q} - \frac{\alpha}{\Delta}\dot q. \tag{10}$$

Our goal is to study linear dynamics of the domain wall in vicinity of the equilibrium position. With this purpose we introduce small deviations in the way $q(t) = q_0 + \tilde q(t)$ and $\Phi(t) = \Phi_0 + \tilde\Phi(t)$. For the limit case $\kappa\Delta_0 \to 0$ the equations of motion (10) linearized with respect to the deviations read

$$(1+\alpha^2)\begin{Vmatrix}\dot{\tilde q}\\ \dot{\tilde\Phi}\end{Vmatrix} \approx \omega_0\ell^2\pi\begin{Vmatrix}0 & \kappa(q_0)\\ \kappa''(q_0) & -\alpha\frac{\kappa(q_0)}{\Delta_0}\end{Vmatrix}\cdot\begin{Vmatrix}\tilde q\\ \tilde\Phi\end{Vmatrix}. \tag{11}$$

For the case of small α the solution of (11) results in harmonic decaying oscillations $\tilde q \propto \sin(\Omega t + \delta_0)e^{-\eta t}$, $\tilde\Phi \propto \cos(\Omega t + \delta_0)e^{-\eta t}$ with frequency

$$\Omega \approx \omega_0\ell^2\pi\sqrt{\kappa(q_0)|\kappa''(q_0)|} \tag{12}$$

and modified effective friction

$$\eta \approx \alpha\omega_0\frac{\pi}{2}\frac{\ell^2\kappa(q_0)}{\Delta_0}. \tag{13}$$

The phase δ_0 is determined by the initial conditions. In (12) and (13) it is taken into account that $\kappa(q_0) > 0$ and $\kappa''(q_0) < 0$ at the maximum point q_0.

It should be noted that an energy expression analogous to (8) was earlier obtained for a certain case of a circular wire segment [24]. However, the circular geometry does not produce any geometrical pinning potential due to the constant curvature $\kappa \equiv$ const, which results in $\Omega = 0$ and undefined q_0. Nevertheless, the domain wall can have an equilibrium position in circular segment in the presence of an external magnetic field [24,25].

In more general case $\Delta_0\kappa \in (0,1)$ the Ansatz (7) leads to the following expressions for the eigenfrequency and effective friction:

$$\Omega = \omega_0\frac{\ell^2}{\Delta_0^2}\sqrt{|\mathcal{AB}|}, \quad \eta = \alpha\omega_0\frac{\ell^2}{\Delta_0^2}\frac{|\mathcal{A}|+\mathcal{B}}{2},$$
$$\mathcal{A} = \Delta_0^2\int_{-\infty}^{+\infty}\frac{\kappa''(s)}{\cosh\frac{s-q_0}{\Delta_0}}ds,$$
$$\mathcal{B} = \int_{-\infty}^{+\infty}\frac{\kappa(s)}{\cosh\frac{s-q_0}{\Delta_0}}ds - \Delta_0\int_{-\infty}^{+\infty}\frac{\kappa^2(s)}{\cosh^2\frac{s-q_0}{\Delta_0}}ds. \tag{14}$$

In this case the equilibrium position q_0 is defined by the equation

$$\int_{-\infty}^{+\infty}\frac{\kappa'(s)}{\cosh\frac{s-q_0}{\Delta_0}}ds = 0 \tag{15}$$

and the equilibrium value of Φ_0 coincides with one defined in (9); for details see Appendix B.

It is important to emphasize that the pinning potential and the corresponding domain wall oscillations have purely exchange origin, while the weak interactions, e.g., the magnetostatic one, contribute mediately via the value of parameter Δ_0.

III. CASE OF PARABOLIC BEND

Let us now check the obtained general results for an example of parabolic wire, whose central line has a form

$$\boldsymbol{\gamma} = x\hat{\boldsymbol{x}} + \kappa_0\frac{x^2}{2}\hat{\boldsymbol{y}}. \tag{16}$$

The wire curvature $\kappa = \kappa_0(1+\kappa_0^2x^2)^{-3/2}$ as a function of natural parameter $s = \kappa_0^{-1}f(\kappa_0 x)$, with $f(\xi) = \frac{1}{2}[\xi\sqrt{1+\xi^2} + \operatorname{arcsinh}(\xi)]$, is shown in Fig. 2(a). It has a single maximum at point $s_0 = 0$ with extreme value $\kappa(s_0) = \kappa_0$.

In accordance with (15) the equilibrium domain wall position is $q_0 = 0$, i.e., the domain wall is located at the extreme point of the bend. The equilibrium phase value Φ_0 is determined by (9); see Fig. 1.

In the narrow domain wall limit $\Delta_0\kappa_0 \to 0$ the eigenfrequency (12) and effective friction read

$$\Omega \approx \omega_0\sqrt{3}\pi(\kappa_0\ell)^2, \quad \eta \approx \alpha\omega_0\pi\ell\kappa_0/4. \tag{17}$$

In order to verify our analytical results we performed two types of numerical simulation: (i) micromagnetic simulations of magnetically soft nanowire (NMAG code); (ii) numerical solution of the Landau-Lifshitz equations for a discrete chain of magnetic moments.

Let us start by considering the magnetically soft wires, whose geometries are determined by (1) and (16). The radius of cross section $R = 5$ nm and length $L = 1$ μm are fixed for all studied samples, while the extreme curvature κ_0 is varied in the range $\kappa_0 \in [0.005, 0.05]$ nm^{-1} with step $\Delta\kappa_0 = 0.005$ nm^{-1}.

Permalloy is chosen as a material with the following parameters: exchange constant $A = 13$ pJ/m, saturation magnetization $M_s = 860$ kA/m, and damping coefficient $\alpha = 0.01$. These parameters result in the exchange length $\ell \approx 3.7$ nm and $\omega_0 = 30.3$ GHz. Thermal effects and anisotropy are neglected.

The magnetization dynamics is studied by means of numerical simulation of the Landau-Lifshitz equation applying the

NMAG code [43], wherein an irregular tetrahedral mesh with cell size about 1.75 nm is used. Only three magnetic interactions were taken into account, namely exchange, magnetostatic, and Zeeman contributions.

The numerical experiment consists of three steps. Initially, we relax the domain wall structure in an over-damped regime ($\alpha = 0.1$) in order to determine the equilibrium values of collective variables: position q_0 and phase Φ_0. The obtained results fully coincide with the prediction (9). To determine the values of q and Φ we extract the curvilinear magnetization components $m_\mathrm{t} = \boldsymbol{m} \cdot \boldsymbol{e}_\mathrm{T}$, $m_\mathrm{n} = \boldsymbol{m} \cdot \boldsymbol{e}_\mathrm{N}$, and $m_\mathrm{b} = \boldsymbol{m} \cdot \boldsymbol{e}_\mathrm{B}$ from the simulation data, and apply fitting with the Ansatz (7). Namely, the position q is determined as a fitting parameter for the function $m_\mathrm{t}(s) = -p \tanh[(s-q)/\Delta]$, then the phase is determined from the equation $\tan\Phi = m_\mathrm{b}(q)/m_\mathrm{n}(q)$.

In the second step we slightly perturb the domain wall phase Φ by applying a weak magnetic field $\boldsymbol{B} = B_0\boldsymbol{e}_z$ perpendicularly to the wire plane, where $B_0 = 25$ mT. After the system relaxation in the applied field $\boldsymbol{B}$ the field is switched off and the magnetization dynamics is simulated for the natural value of the damping coefficient (the third step). Since the variables Φ and q are canonically conjugated, see Eqs. (10), the perturbed dynamics of Φ induces the dynamics of q, i.e., the domain wall starts to move (see Supplemental Material [44]). Typical time dependences of these collective variables are shown in Figs. 2(b) and 2(c), where one can see harmonic decaying oscillations with well pronounced frequency Ω and friction parameter η. In this way we determine Ω and η for all range of the studied curvatures κ_0. The frequency Ω as well as the friction η increases with the curvature increasing; see Fig. 3 (round markers). One should note a good agreement of the obtained numerical results with the analytical prediction (14) with $\Delta_0 = 2\ell$; see solid lines in Fig. 3 and Appendix B for details. This means that the approximation of magnetostatic interaction by the effective easy-tangential anisotropy is physically sound for a domain wall dynamics in the thin nanowires.

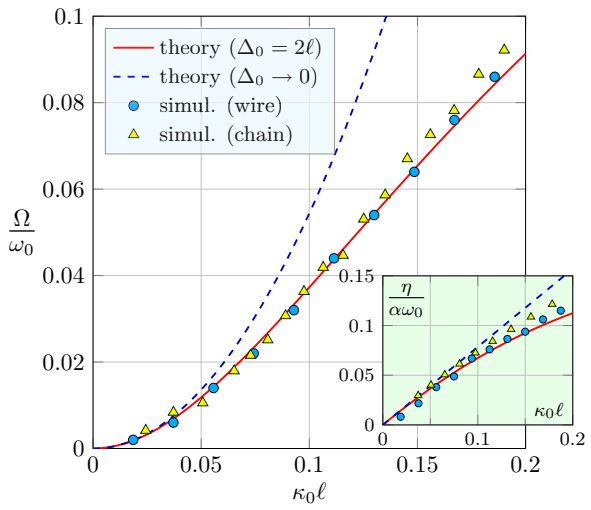

FIG. 3. (Color online) Eigenfrequency of the domain wall oscillations in vicinity of the equilibrium—the extreme point of parabolic bend; see Fig. 1. Solid and dashed lines correspond to the predictions (14) and its narrow-wall asymptotics (17), respectively. Markers show the results of numerical simulations for nanowires (disks) and discrete chains of magnetic moments (triangles). The inset demonstrates dependence of the effective friction on the curvature parameter.

Additionally, we study dynamics of discrete chains of magnetic moments $\boldsymbol{m}_i$, with $i = \overline{1,N}$, aligned along parabolic line (16). The moments are aligned equidistantly with the fixed step size Δs along the chain. As previously, only three magnetic interactions are taken into account, namely exchange (with $\ell = 3\Delta s$), dipole-dipole, and Zeeman contribution. Total number of moments is fixed $N = 76$, while the curvature parameter κ_0 is varied but the restriction $\kappa_0\Delta s \ll 1$. Dynamics of this system is described by a set of N vector Landau-Lifshitz equations which are solved by means of common numerical methods; in details this procedure is described in Ref. [45].

The domain wall oscillations are studied in the same way as for the wires described above. The resulting eigenfrequencies and friction parameters are shown in Fig. 3 by triangles.

In conclusion, we demonstrate an effect of curvature-induced pinning of a transversal head-to-head (tail-to-tail) domain wall at a local wire bend. The curvature-induced pinning potential has purely exchange origin. We obtain an expression (14) for frequency and effective friction of the free domain wall oscillations within the pinning potential, and we demonstrate its validity numerically for the range of parameters $\kappa\Delta \sim 10^{-1}$. For the case of a narrow domain wall or weak curvature ($\kappa\Delta \sim 10^{-2}$) the approximations (12) and (13) can be used. The good agreement of analytical predictions and results of full scale numerical simulations for magnetically soft cases ($K = 0$) demonstrates that the approximation of magnetostatic interaction by the effective easy-tangential anisotropy is physically sound for a domain wall dynamics in the thin nanowires.

ACKNOWLEDGMENTS

The present work was partially supported by the Program of Fundamental Research of the Department of Physics and Astronomy of the National Academy of Sciences of Ukraine (Project No. 0112U000056).

APPENDIX A: STATIC SOLUTIONS FOR A PLANAR WIRE

Static form of Eqs. (3) reads $\delta\mathcal{E}/\delta\theta = 0$ and $\delta\mathcal{E}/\delta\phi = 0$. Taking into account form of energy (4) and exchange energy density (5) one obtains the following set of equations:

$$\theta'' - \sin\theta\,\cos\theta[\phi'^2 - \kappa^2\sin^2\phi + w^{-2}] - 2\phi'\kappa\,\sin^2\theta + \kappa'\cos\phi = 0, \tag{A1a}$$

$$\phi'' + 2\theta'[\cot\theta\phi' + \kappa\,\sin\phi] + \kappa^2\sin\phi\,\cos\phi - \kappa'\cot\theta\,\sin\phi = 0. \tag{A1b}$$

Equation (A1b) has solutions $\phi = \phi_0 = 0, \pi$. Substitution of this solution into (A1a) results in Eq. (6), which determines the function $\theta(s)$.

APPENDIX B: DETAILS OF THE q–Φ MODEL USAGE

The equations of motion (3) are the Euler-Lagrange equations

$$\frac{\delta\mathcal{L}}{\delta\xi_i} - \frac{d}{dt}\frac{\delta\mathcal{L}}{\delta\dot{\xi}_i} = \frac{\delta\mathcal{F}}{\delta\dot{\xi}_i}, \quad \xi_i \in \{\theta,\phi\} \tag{B1}$$

for Lagrange function [46]

$$\mathcal{L} = -\frac{\mathcal{S}}{\omega_0}\int_{-\infty}^{\infty}\phi\,\sin\theta\,\dot{\theta}\,ds - \mathcal{E} \tag{B2}$$

and dissipative function

$$\mathcal{F} = \frac{\alpha}{2}\mathcal{S}\int_{-\infty}^{\infty}[\dot{\theta}^2 + \sin^2\theta\dot{\phi}^2]ds. \tag{B3}$$

Substituting the Ansatz (7) into (B2) and (B3) and performing the integration over s (along the curve) one obtains the effective Lagrange and effective dissipative functions in the form

$$\mathcal{L}_{\text{eff}} = \frac{2\mathcal{S}}{\omega_0}\Phi\dot{q} - \mathcal{E}, \quad \mathcal{F}_{\text{eff}} = \alpha\frac{\mathcal{S}}{\omega_0}\left[\frac{\dot{q}^2}{\Delta} + \Delta\dot{\Phi}^2\right]. \tag{B4}$$

The Euler-Lagrange equations (B1) written for the effective Lagrange and dissipative functions (B4) and for $\xi_i \in \{q,\Phi\}$ result in the equations of motion (10).

Let us now consider energy of the system $\mathcal{E}$. Substituting the Ansatz (7) into the energy expression (4) and performing the integration one obtains (up to an additive constant)

$$\frac{\mathcal{E}}{2\mathcal{S}} = \frac{\ell^2}{\Delta} + \Delta k_t + \frac{\ell^2}{\Delta^2}\left[pF_1\cos\Phi - \frac{F_2}{2}\sin^2\Phi\right],$$
$$F_n = \int_{-\infty}^{\infty} f^n(s)ds, \quad f(s) = \frac{\kappa(s)\Delta}{\cosh\frac{s-q}{\Delta}}. \tag{B5}$$

In the limit case $\kappa\Delta \to 0$ the expression (B5) is reduced to (8). For the more general case $0 < \Delta\kappa < 1$ one has $f < 1$ and consequently $F_1 > F_2$. In this case the value of phase Φ_0 which minimizes the energy (B5) is determined as $\cos\Phi_0 = -p$ and the corresponding value of the equilibrium domain wall position q_0 is determined by Eq. (15). The case $\Delta\kappa > 1$ (domain wall width is larger than the curvature radius) is not considered here, because the application of the Ansatz (7) is questionable in this case and a precise solution of Eq. (6) is required.

The equations of motion linearized in the vicinity of the equilibrium $q = q_0$, $\Phi = \Phi_0$ read

$$(1+\alpha^2)\begin{Vmatrix}\dot{\tilde{q}}\\ \dot{\tilde{\Phi}}\end{Vmatrix} = \omega_0\frac{\ell^2}{\Delta_0^2}\begin{Vmatrix}\alpha\mathcal{A} & \Delta_0\mathcal{B}\\ \frac{\mathcal{A}}{\Delta_0} & -\alpha\mathcal{B}\end{Vmatrix}\cdot\begin{Vmatrix}\tilde{q}\\ \tilde{\Phi}\end{Vmatrix}, \tag{B6}$$

where $\tilde{q} = q - q_0$ and $\tilde{\Phi} = \Phi - \Phi_0$ are small deviations from the equilibrium and quantities $\mathcal{A}$ and $\mathcal{B}$ are defined in (14). For the case of small α the solution of (B6) results in harmonic decaying oscillations $\tilde{q} \propto \sin(\Omega t + \delta_0)e^{-\eta t}$, $\tilde{\Phi} \propto \cos(\Omega t + \delta_0)e^{-\eta t}$ with frequency Ω and effective friction η presented in (14).

For the case of parabolic wire (16) one obtains $\mathcal{A} = \mathcal{A}(\Delta_0\kappa_0)$ and $\mathcal{B} = \mathcal{B}(\Delta_0\kappa_0)$, where

$$\mathcal{A}(x) = 3x^2\int_{-\infty}^{+\infty}\frac{(5\xi^2-1)\operatorname{sech}\frac{f(\xi)}{x}}{(1+\xi^2)^4}d\xi,$$
$$\mathcal{B}(x) = \int_{-\infty}^{\infty}\left[1 - x\frac{\operatorname{sech}\frac{f(\xi)}{x}}{(1+\xi^2)^{\frac{3}{2}}}\right]\frac{\operatorname{sech}\frac{f(\xi)}{x}}{1+\xi^2}d\xi. \tag{B7}$$

These expressions are used to calculate the eigenfrequencies and friction parameters in (14); see solid lines in Fig. 3.

[1] S. S. P. Parkin, M. Hayashi, and L. Thomas, Magnetic domain-wall racetrack memory, Science **320**, 190 (2008).

[2] M. Hayashi, L. Thomas, R. Moriya, C. Rettner, and S. S. P. Parkin, Current-controlled magnetic domain-wall nanowire shift register, Science **320**, 209 (2008).

[3] D. A. Allwood, G. Xiong, M. D. Cooke, C. C. Faulkner, D. A. N. Vernier, and R. P. Cowburn, Submicrometer ferromagnetic NOT gate and shift register, Science **296**, 2003 (2002).

[4] D. A. Allwood, G. Xiong, C. C. Faulkner, D. Atkinson, D. Petit, and R. P. Cowburn, Magnetic domain-wall logic, Science **309**, 1688 (2005).

[5] P. Xu, K. Xia, C. Gu, L. Tang, H. Yang, and J. Li, An all-metallic logic gate based on current-driven domain wall motion, Nat. Nanotechnol. **3**, 97 (2008).

[6] G. Catalan, J. Seidel, R. Ramesh, and J. F. Scott, Domain wall nanoelectronics, Rev. Mod. Phys. **84**, 119 (2012).

[7] E. R. Lewis, D. Petit, L. Thevenard, A. V. Jausovec, L. O'Brien, D. E. Read, and R. P. Cowburn, Magnetic domain wall pinning by a curved conduit, Appl. Phys. Lett. **95**, 152505 (2009).

[8] S. Glathe and R. Mattheis, Magnetic domain wall pinning by kinks in magnetic nanostripes, Phys. Rev. B **85**, 024405 (2012).

[9] D. M. Burn, M. Chadha, S. K. Walton, and W. R. Branford, Dynamic interaction between domain walls and nanowire vertices, Phys. Rev. B **90**, 144414 (2014).

[10] M. Kläui, C. A. F. Vaz, J. Rothman, J. A. C. Bland, W. Wernsdorfer, G. Faini, and E. Cambril, Domain Wall Pinning in Narrow Ferromagnetic Ring Structures Probed by Magnetoresistance Measurements, Phys. Rev. Lett. **90**, 097202 (2003).

[11] M. Kläui, H. Ehrke, U. Rüdiger, T. Kasama, R. E. Dunin-Borkowski, D. Backes, L. J. Heyderman, C. A. F. Vaz, J. A. C. Bland, G. Faini *et al.*, Direct observation of domain-wall pinning at nanoscale constrictions, Appl. Phys. Lett. **87**, 102509 (2005).

[12] M. Hayashi, L. Thomas, C. Rettner, R. Moriya, X. Jiang, and S. S. P. Parkin, Dependence of Current and Field Driven Depinning of Domain Walls on Their Structure and Chirality in Permalloy Nanowires, Phys. Rev. Lett. **97**, 207205 (2006).

[13] D. Bedau, M. Klaui, S. Krzyk, U. Rudiger, G. Faini, and L. Vila, Detection of Current-Induced Resonance of Geometrically Confined Domain Walls, Phys. Rev. Lett. **99**, 146601 (2007).

[14] D. Atkinson, D. S. Eastwood, and L. K. Bogart, Controlling domain wall pinning in planar nanowires by selecting domain wall type and its application in a memory concept, Appl. Phys. Lett. **92**, 022510 (2008).

[15] L. K. Bogart, D. Atkinson, K. O'Shea, D. McGrouther, and S. McVitie, Dependence of domain wall pinning potential landscapes on domain wall chirality and pinning site geometry in planar nanowires, Phys. Rev. B **79**, 054414 (2009).

[16] D. Petit, H. T. Zeng, J. Sampaio, E. Lewis, L. O'Brien, A.-V. Jausovec, D. Read, R. P. Cowburn, K. J. O'Shea, S. McVitie *et al.*, Magnetic imaging of the pinning mechanism of asymmetric transverse domain walls in ferromagnetic nanowires, Appl. Phys. Lett. **97**, 233102 (2010).

[17] J.-S. Kim, M.-A. Mawass, A. Bisig, B. Krüger, R. M. Reeve, T. Schulz, F. Büttner, J. Yoon, C.-Y. You, M. Weigand, H. Stoll, G. Schütz, H. J. M. Swagten, B. Koopmans, S. Eisebitt, and M. Kläui, Synchronous precessional motion of multiple domain walls in a ferromagnetic nanowire by perpendicular field pulses, Nat. Commun. **5**, 3429 (2014).

[18] Y. Nakatani, A. Thiaville, and J. Miltat, Faster magnetic walls in rough wires, Nat. Mater. **2**, 521 (2003).

[19] A. Thiaville, Y. Nakatani, J. Miltat, and N. Vernier, Domain wall motion by spin-polarized current: a micromagnetic study, J. Appl. Phys. **95**, 7049 (2004).

[20] A. Thiaville, Y. Nakatani, J. Miltat, and Y. Suzuki, Micromagnetic understanding of current-driven domain wall motion in patterned nanowires, Europhys. Lett. **69**, 990 (2005).

[21] A. A. Ivanov and V. A. Orlov, A comparative analysis of the mechanisms of pinning of a domain wall in a nanowire, Phys. Solid State **53**, 2441 (2011).

[22] V. Uhlíř, S. Pizzini, N. Rougemaille, J. Novotný, V. Cros, E. Jiménez, G. Faini, L. Heyne, F. Sirotti, C. Tieg, A. Bendounan, F. Maccherozzi, R. Belkhou, J. Grollier, A. Anane, and J. Vogel, Current-induced motion and pinning of domain walls in spin-valve nanowires studied by XMCD-PEEM, Phys. Rev. B **81**, 224418 (2010).

[23] T. Gerhardt, A. Drews, and G. Meier, Controlled pinning and depinning of domain walls in nanowires with perpendicular magnetic anisotropy, J. Phys.: Condens. Matter **24**, 024208 (2011).

[24] B. Krüger, D. Pfannkuche, M. Bolte, G. Meier, and U. Merkt, Current-driven domain-wall dynamics in curved ferromagnetic nanowires, Phys. Rev. B **75**, 054421 (2007).

[25] M. Jamali, K.-J. Lee, and H. Yang, Effect of nonadiabatic spin transfer torque on domain wall resonance frequency and mass, Appl. Phys. Lett. **98**, 092501 (2011).

[26] D. D. Sheka, V. P. Kravchuk, and Y. Gaididei, Curvature effects in statics and dynamics of low dimensional magnets, J. Phys. A: Math. Theor. **48**, 125202 (2015).

[27] *Spin Dynamics in Confined Magnetic Structures III*, edited by B. Hillebrands and A. Thiaville, Topics in Applied Physics Vol. 101 (Springer, Berlin, 2006).

[28] D. G. Porter and M. J. Donahue, Velocity of transverse domain wall motion along thin, narrow strips, J. Appl. Phys. **95**, 6729 (2004).

[29] V. V. Slastikov and C. Sonnenberg, Reduced models for ferromagnetic nanowires, IMA J. Appl. Math. **77**, 220 (2012).

[30] V. P. Kravchuk, Stability of magnetic nanowires against spin-polarized current, Ukr. J. Phys. **59**, 1001 (2014).

[31] J. C. Slonczewski, Dynamics of magnetic domain walls, Int. J. Magn. **2**, 85 (1972).

[32] A. A. Thiele, Steady-State Motion of Magnetic Domains, Phys. Rev. Lett. **30**, 230 (1973).

[33] A. P. Malozemoff and J. C. Slonzewski, *Magnetic Domain Walls in Bubble Materials* (Academic Press, New York, 1979).

[34] A. Thiaville, J. Garcia, and J. Miltat, Domain wall dynamics in nanowires, J. Magn. Magn. Mater. **242–245**, 1061 (2002).

[35] A. Mougin, M. Cormier, J. P. Adam, P. J. Metaxas, and J. Ferré, Domain wall mobility, stability and Walker breakdown in magnetic nanowires, Europhys. Lett. **78**, 57007 (2007).

[36] A. V. Khvalkovskiy, K. A. Zvezdin, Y. V. Gorbunov, V. Cros, J. Grollier, and A. K. Zvezdin, High Domain Wall Velocities due to Spin Currents Perpendicular to the Plane, Phys. Rev. Lett. **102**, 067206 (2009).

[37] P. Landeros and A. S. Núñez, Domain wall motion on magnetic nanotubes, J. Appl. Phys. **108**, 033917 (2010).

[38] A. Thiaville, S. Rohart, É. Jué, V. Cros, and A. Fert, Dynamics of Dzyaloshinskii domain walls in ultrathin magnetic films, Europhys. Lett. **100**, 57002 (2012).

[39] J. Otálora, J. López-López, P. Vargas, and P. Landeros, Chirality switching and propagation control of a vortex domain wall in ferromagnetic nanotubes, Appl. Phys. Lett. **100**, 072407 (2012).

[40] J. A. Otálora, J. A. López-López, P. Landeros, P. Vargas, and A. S. Núñez, Breaking of chiral symmetry in vortex domain wall propagation in ferromagnetic nanotubes, J. Magn. Magn. Mater. **341**, 86 (2013).

[41] V. P. Kravchuk, Influence of Dzialoshinskii-Moriya interaction on static and dynamic properties of a transverse domain wall, J. Magn. Magn. Mater. **367**, 9 (2014).

[42] P. Bruno, Geometrically Constrained Magnetic Wall, Phys. Rev. Lett. **83**, 2425 (1999).

[43] T. Fischbacher, M. Franchin, G. Bordignon, and H. Fangohr, A systematic approach to multiphysics extensions of finite-element-based micromagnetic simulations: Nmag, IEEE Trans. Magn. **43**, 2896 (2007).

[44] See Supplemental Material at http://link.aps.org/supplemental/10.1103/PhysRevB.92.104412 for the supplemental video.

[45] D. D. Sheka, V. P. Kravchuk, K. V. Yershov, and Y. Gaididei, Torsion-induced effects in magnetic nanowires, Phys. Rev. B **92**, 054417 (2015).

[46] W. Döring, Über die Trägheit der Wände zwischen Weißschen Bezirken, Z. Naturforsch. A **3**, 373 (1948).